Planetary-Scale Inertio Gravity Waves in the Numerical Spectral Model

H. G. Mayr, J. G. Mengel, E. R. Talaat, H. S. Porter

Popular Summary:

In the polar region of the upper mesosphere, horizontal wind oscillations have been observed with periods around 10 hours. Waves with such a period are generated in our Numerical Spectral Model (NSM), and they are identified as planetary-scale inertio gravity waves (IGW). These IGWs have periods between 9 and 11 hours and appear above 60 km in the zonal mean (m = 0), as well as in zonal wavenumbers m = 1 to 4. The waves can propagate eastward and westward and have vertical wavelengths around 25 km. The amplitudes in the wind field are typically between 10 and 20 m/s and can reach 30 m/s in the westward propagating component for m = 1 at the poles. In the temperature perturbations, the wave amplitudes above 100 km are typically 5 K and as large as 10 K for m = 0 at the poles. The IGWs are intermittent but reveal systematic seasonal variations, with the largest amplitudes occurring generally in late winter and spring. In the NSM, the IGW are generated like the planetary waves (PW). They are produced apparently by the instabilities that arise in the zonal mean circulation. Relative to the PWs, however, the IGWs propagate zonally with much larger velocities, such that they are not affected much by interactions with the background zonal winds. Since the IGWs can propagate through the mesosphere without much interaction, except for viscous dissipation, one should then expect that they reach the thermosphere with significant and measurable amplitudes.

Planetary-Scale Inertio Gravity Waves in the Numerical Spectral Model

H. G. Mayr[1], J. G. Mengel[2], E. R. Talaat[3], H. S. Porter[4]
[1]Goddard Space Flight Center, Greenbelt, MD, 20771
[2]Science Systems & Applications, Inc., Lanham, MD
[3]Applied Physics Laboratory, Johns Hopkins University, Laurel, MD
[4]Furman University, Greenville, SC

Prepared for Publication
in
Annales Geophysicae

December 2003

Abstract: In the polar region of the upper mesosphere, horizontal wind oscillations have been observed with periods around 10 hours. Waves with such a period are generated in our Numerical Spectral Model (NSM), and they are identified as planetary-scale inertio gravity waves (IGW). These IGWs have periods between 9 and 11 hours and appear above 60 km in the zonal mean (m = 0), as well as in m = 1 to 4 propagating eastward and westward. Under the influence of the Coriolis force, the amplitudes of the waves propagating westward are larger at high latitudes than those of the eastward waves. The waves grow in magnitude at least up to about 100 and have vertical wavelengths around 25 km. Applying a window of 15 days, the amplitudes in the wind field are typically between 10 and 20 m/s and can reach 30 m/s in the westward propagating component for m = 1 at the poles. In the temperature perturbations, the wave amplitudes above 100 km are typically 5 K and as large as 10 K for m = 0 at the poles. The IGWs are intermittent but reveal systematic seasonal variations, with the largest amplitudes occurring generally in late winter and spring. Numerical experiments show that the waves are also generated without excitation of the migrating tides. The waves and their seasonal variations then are different. But their amplitudes and periodicities are similar, indicating that the tides are not essential to generate the waves. The IGW are generated in the NSM like the planetary waves (PW) - they are produced apparently by the instabilities that arise in the zonal mean circulation. When the solar heating is turned off for m = 0, both the PWs and IGWs essentially disappear. That the IGWs and PWs in the NSM have common roots is also apparent from the striking similarity of their seasonal variations that is documented in the paper. The distinguishing difference however is that, relative to the PWs, the planetary-scale IGWs discussed here propagate zonally with much larger velocities. In contrast to the PWs, the IGWs thus are not affected much by interactions with the background zonal winds that vary drastically with season in the mesosphere. Since the IGWs can propagate through the mesosphere without much interaction, except for viscous dissipation, one should expect that they reach the thermosphere with measurable amplitudes.

I. Introduction

Hernandez et al. (1992) reported evidence for the existence of a pronounced westward propagating wave with a period of 10.1 hours in the southern hemisphere near the pole. The data for this analysis were based on optical measurements derived from Doppler shifting and broadening of OH emissions at altitudes near 90 km, which yielded winds and temperatures respectively. Medium frequency radar

measurements from the Scott Base at 78°S (Fraser, 1984) provided additional observations of horizontal winds. The measurements were carried out during austral winter in August 1991. During the period of observations, and at both stations, the 10-hour wave was apparent in the wind data. In the optical measurements, the wave dominated at the South Pole where a wind amplitude of 8 m/s was inferred at the 95% significance level. The wave was also seen with the radar at 78°S, but the semi-diurnal tide dominated there.

Horizontal winds at the pole must be associated with zonal wavenumber m = 1, and the phase progression of the observed 10-hour oscillation revealed that the wave was propagating westward (Hernandez et al., 1992). The related temperature variations for this wavenumber should vanish at the pole, and the analysis showed that for the observed periodicity in the winds.

Hernandez et al. (1993) again observed the 10-hour wave during the southern winter of 1992 in the Antarctic polar region, but in this case it was accompanied by a westward propagating 12-hour wave of comparable magnitude they called an inertio gravity wave. Forbes et al. (1995) also observed the westward propagating 12-hour wave in radar measurements near the North Pole and classified it as a non-migrating semi-diurnal tide.

In a recent paper (Mayr et al., 2003), we reported that our model produces in the upper mesosphere waves with periods around 10 hours such as observed by Hernandez et al. (1992, 1993). The oscillations were identified as planetary-scale inertio gravity waves (IGW), which are distinctly different from the non-migrating semi-diurnal tide that is also generated in the model. It is the purpose of the present paper to describe more fully the wave oscillations in the temperature and wind fields generated in the model and in particular to elucidate their distinct seasonal variations.

II. Numerical Spectral Model

The design of the Numerical Spectral Model (NSM) was introduced by Chan et al. (1994), and we applied 2D and 3D versions of this model to study some aspects of the middle atmosphere dynamics (Mengel et al., 1994; Mayr et al., 1997, 2001a, b, 2003). The model has been discussed in the literature and is briefly reviewed here for completeness.

The NSM is non-linear and time dependent. Formulated with spherical harmonics, the NSM delineates the dynamical components in terms of zonal wavenumbers: m = 0 for the zonal mean that includes the Semiannual Oscillation (SAO) and Quasi-biennial Oscillation (QBO), and m = 1 to 4 for the tides and planetary waves. The Navier Stokes equations are solved to describe the variations

around the global mean of temperature and density, covering the atmosphere from the ground up to 400 km (240 km in the present application to speed up computation). By marching in time, the equations are solved for the spherical harmonics, and their synthesis provides the solution. The non-linear terms are evaluated in physical space. The NSM is run with a vertical step size of about 0.5 km (below 120 km) and a time step of about 5 minutes. The maximum meridional and zonal wavenumbers are respectively n = 12 (12 Gaussian point per hemisphere) and m = 4 (16 points in longitude).

For the zonal mean (m = 0), the heat source is due to UV radiation in the mesosphere and stratosphere taken from Strobel (1978) and due to EUV radiation in the thermosphere. The heating rates for the solar driven migrating tides in the middle atmosphere and troposphere are taken from Forbes and Garrett (1978). The radiative loss in the model is described in terms of Newtonian cooling, for which we adopted the cooling parameterization of Zhu (1989).

The 3D version of the NSM discussed here differs from earlier applications published in the literature in that we incorporate tropospheric heating for the zonal mean (m = 0) to reproduce qualitatively the observed zonal jets and temperature variations near the tropopause. We had earlier applied such a source in our 2D model to study its effect on the QBO, and we find that it affects also the planetary waves significantly.

The NSM incorporates the Doppler Spread Parameterization (DSP) for small-scale gravity waves (GW) formulated by Hines (1997a, b). The DSP deals with a spectrum of waves that interact with each other to produce Doppler spreading, which affects the interaction of the waves with the background flow. The DSP has been applied also successfully in a number of other models (e.g., Akmaev, 2001; Manzini et al., 1997).

In the NSM, the GW source at the initial height (for the present model taken to be 7.5 km) is assumed to be isotropic and independent of latitude and season. The DSP assures conservation of GW momentum (and energy), and this requires at each altitude, latitude and longitude that a system of nonlinear equations is solved involving GW parameters, background winds, and buoyancy frequency. The equations are solved with Newtonian iteration, and convergence is assured by adjusting the time integration step. With an adjustable parameterization factor, the DSP also provides height dependent eddy diffusion rates (isotropic), which are incorporated into the NSM under the assumption that the variations with latitude and season can be ignored for simplicity. The heating rates associated with the dissipation of GWs are not accounted for.

III. Model Results

III. 1. Wave Patterns and Global Survey

Horizontal winds at the poles must have zonal wavenumber m = 1. We show then with Figure 1 contour plots of the computed meridional winds in the polar region at 84°N (a) and 77 °N (b) for this wavenumber covering the altitude range between 80 and 110 km. The winds are presented for a period of 4 days in March of the 3rd model year, during a time when relatively large waves are generated with evident periodicity close to 10 hours as identified in two cases. With contour intervals of 10 m/s, the amplitudes are generally well above 20 m/s and grow with height. Although the waves are highly variable, the pattern indicates upward propagation with vertical wavelengths of about 20 km. Our analysis shows that the waves at polar latitudes mainly propagate westward and thus reproduce an important aspect of the observations by Hernandez et al. (1992) who had inferred that for their 10-hour oscillation.

Temperature variations at the poles must have zonal wavenumber m = 0. Analogous to Figure 1, we present with Figure 2 the computed temperature perturbations for this wavenumber at 84°N (a) and 70 °N (b) covering the same altitude range and time span. The displayed wave periods (from zero crossings) are between 9 and 10 hours, the vertical wavelengths are typically around 20 km, and the amplitudes often exceed 5 K and tend to grow with altitude.

For m = 0, wave patterns in temperature should be associated energetically with meridional (irrotational) wind oscillations, which we present in Figure 2c for a latitude of 77°N. With a contour interval of 4 m/s, the computed winds reach amplitudes exceeding 30 m/s and indeed reveal periods close to those apparent from the temperature perturbations. And the vertical wavelengths are again close to 20 km.

The above model results were displayed for selected zonal wavenumbers, m = 1 for meridional winds, and m = 0 for temperature perturbations, which are appropriate to highlight the conditions at high latitudes. The overall patterns, however, would not be very different if we displayed in Figures 1 and 2 the results for the combined wavenumbers m = 0 to 4 retained in the model, except that the variability and maximum amplitudes would be larger away from the poles.

Anticipating results later discussed that reveal distinct seasonal variations, we present in Figures 3 and 4, for the meridional winds and temperature perturbations respectively, the maximum amplitudes of the stationary wave (a) and the eastward (b, c) and westward (d, e) propagating waves with periods between 9 and 10.5 hours derived for a running window of 15 days from the time span 26 to 29 months

(March through May). This shows that waves below 12 hours are generated in our model for m = 0 to 2, and for m = 3 and 4 as well (not presented). Both eastward and westward propagating waves are produced. For the time span and range of periods analyzed, the m = 1 westward propagating component in the meridional winds is largest with a peak of 25 m/s near 100 km, and it peaks apparently in the northern polar region. With a maximum amplitude of 19 m/s near 75°N, the stationary (non-migrating) wave for m = 0 is also prominent as the results in Figure 2c already indicated. The asymmetry between the northern and southern hemispheres, evident in all the wavenumbers and in the eastward and westward propagating waves, clearly indicates that the amplitudes are much larger during summer than winter months.

In many respects, as expected, the wave patterns for the temperature perturbations in Figure 4 are similar to those in the meridional winds just discussed. The difference is that the largest amplitudes occur in the polar region for m = 0, which approach 10 K at 110 km in the summer hemisphere. In the other wavenumbers, the temperature amplitudes are close to 5 K.

The above results describe the maximum amplitudes extracted from a time span of 3 months, when the Sun is moving from the southern into the northern hemisphere. With a running window of 15 days applied in the analysis, the recorded amplitudes represent more than 30 cycles for waves with periods around 10 hours. This implies that the waves generated in the NSM are persistent at times -- and then have substantial wind and temperature amplitudes that should be measurable.

III.2. Spectral Analysis

To provide further details about the waves discussed here, we present in Figures 5 and 6 the amplitude spectra for the meridional winds and temperature perturbations. For the wavenumbers m = 0 (a), 1 (b) and 2 (c), the spectra are displayed at 100 km altitude as functions of latitude, covering periods between 8 and 14 hours. The stationary waves (m = 0) are shown in gray scales, and the westward and eastward waves in red and blue respectively. To eliminate clutter, the lowest 40% or 50% of contours are suppressed. As for Figures 3 and 4, a running window of 15 days was applied in the analysis, and the time span covered the months March through May (i.e., late northern winter and spring). The spectra for each of the wavenumbers displayed contain several wave periods with prominent amplitudes. But these waves are generally not excited simultaneously.

The meridional winds for the m = 0 waves (Figure 5a) show a peak with 17 m/s near 75°N with a period close to 9 hours. Such a wave also appears in the temperature perturbations (Figure 6a) that peak in the Arctic exceeding 5 K, which is consistent with the results presented in Figure 2. In the

temperatures there is also a stationary semi-diurnal 12-hour tide (generated in the NSM exclusively by non-linear coupling between migrating tide and planetary waves), which apparently does not produce a meridional wind oscillation that is large enough to appear in the truncated contours of Figure 5a.

In Figure 5b, the non-migrating 12-hour tide for m = 1 dominates in the polar regions with a maximum amplitude close to 40 m/s (at 100 km), and it is shown propagating westward. This tide is produced in the NSM with planetary waves, at least partially, as Forbes et al. (1995) had proposed on the basis of radar measurements. The corresponding westward temperature tide (Figure 6b) reaches amplitudes exceeding 5 K at high latitudes in the northern hemisphere and amplitudes close to 4 K at equatorial latitudes. For the present paper, the waves of principal interest appear in the amplitude maxima with periods close to 10 and 9 hours, which are shown both in the meridional winds (Figure 5b) and in the temperature perturbations (Figure 6b). For the 3-months time span, the westward propagating 10-hour wave in the northern hemisphere is seen to be weaker than the non-migrating semi-diurnal tide, but it still reaches amplitudes close to 24 m/s at 84° latitude and even larger values at the pole. For a more limited time span in March of the 3rd model year, we had shown (Mayr et al., 2003) that the amplitude of the 10-hour wave exceeded that of the semi-diurnal tide -- which is not a typical situation but it is similar to the scenario Heranandez et al. (1992) had encountered. Waves with periods close to 9-hours are shown in Figures 5b and 6b, and they propagate eastward. In contrast to the m = 1 westward waves that clearly tend to peak at the poles, the much weaker eastward waves apparently do not extend with significant amplitudes into the polar region.

For m = 2, Figures 5c and 6c show the large westward migrating 12-hour semi-diurnal tide that is produced by solar heating, with amplitude maxima close to 50 m/s in the winds and more than 15 K in the temperature variations (variable contour intervals are used to describe these features). In the northern hemisphere, a westward propagating wave appears in the meridional winds with amplitude close to 10 m/s, which has a period close to 10 hours (Figure 5c). The corresponding temperature oscillation has a small amplitude of about 2 K (Figure 6c). Compared with the westward propagating waves, the eastward waves occupy lower latitudes for m = 2, as is the case for m = 1. The eastward waves for the meridional winds, at low to mid latitudes, have amplitudes approaching 10 m/s with periods close to 9 and 11 hours – and the related temperature amplitudes are about 3 K.

To reveal the nature of the waves discussed here, we present in Figure 7 contour plots of snap-shots for the eastward (a) and westward (b) propagating components. For a time span chosen to contain waves of some period with relatively large amplitude, an analysis is performed to extract the average wave characteristics, i.e., phase and amplitude as functions of altitude and latitude, delineating the

eastward and westward components. In the present case, we have chosen a time span in mid September of the 3rd model year when pronounced waves with 9-hour periodicity are generated in the southern hemisphere. The patterns described in Figure 7, considered representative of the waves discussed, show that the horizontal wavelength is about 40° in latitude and that the latitudinal variations for the eastward and westward propagating waves differ significantly as seen already from Figures 3 through 6. The waves are presented in 3-hour intervals, indicating downward phase progression with a vertical wavelength of about 25 km, which is similar to that shown in Figures 1 and 2. The wave patterns shown here reveal a relationship between meridional wave number and vertical wavelength that lends support to our interpretation (Mayr et al., 2003) that the waves are planetary scale inertio gravity waves (IGW) related to the Class I waves discussed in the classical literature (Longuett Higgins, 1968).

III.3. Seasonal Variations and Wave Genesis

The IGWs discussed exhibit pronounced seasonal variations as shown in Figures 8 and 9 respectively for the meridional winds and temperature variations at 100 km altitude. With a running window of 15 days, we extracted the waves with periods between 9 and 10.5 hours. The amplitudes for m = 0 (a) and m = 1 propagating eastward (b) and westward (c) are plotted versus latitude and time covering 24 months. In both hemispheres, these wave components tend to be excited preferentially during winter months, beginning in late fall and extending into spring. Consistent with the results shown earlier, the westward propagating waves for the meridional winds with wavenumber m = 1 are largely confined to high latitudes. The eastward propagating waves in contrast do not extend with significant amplitudes into the polar regions but instead extend to low latitudes and across the equator. These patterns are characteristic of the seasonal and latitudinal variations throughout the mesosphere above 50 km.

In the temperature variations (Figure 9), the waves with m = 0 (a) are largest at polar latitudes. Consistent with the waves in the meridional winds for m = 1, the corresponding temperature amplitudes for the westward component are largest at high latitudes (Figure 9c), but they vanish at the poles. And the eastward waves (Figure 9b) extend with substantial amplitudes (almost 5K) towards equatorial latitudes.

The wave patterns for m = 2, 3 and 4 (not presented) reveal similar trends in the seasonal variations: the amplitudes tend to be largest during winter months approaching spring.

We have carried out numerical experiments that could shed some light on the possible excitation mechanism for the waves. When the sources for the solar (thermal) migrating diurnal and semi-diurnal tides are turned off, the waves are still excited as shown in Figure 10 for the meridional winds with m = 1. Compared to Figures 8b and 8c, the waves are different as seen in their seasonal variations. Their amplitudes however are of comparable magnitude (about 25 m/s maximum westward and 12 m/s eastward), which leads us to the conclusion that the migrating tides are not essential to generate the waves. That the tides do influence the waves is not surprising, considering the interactions that couple the dynamical features of the atmosphere in part through gravity wave filtering, as our modeling studied have shown.

The waves are generated like the planetary waves (PW) in our model. When the solar heating that drives the zonal mean (m = 0) circulation and related temperature and pressure variations is turned off, the waves essentially disappear. Like the planetary waves (PW), the waves are apparently generated through the instabilities that arise in the zonal mean circulation. This picture is supported by the computed seasonal variations of the meridional winds at 60 km for m = 1 and 3 (as well as m = 2 and 4, not shown), which closely resemble those seen in the waves (Figure 8). In both hemispheres, at this altitude, the PWs are preferentially excited during the winter and spring season. In contrast to the IGWs discussed here, the seasonal variations of the PWs change as they propagate into the upper mesosphere. With their longer oscillation periods, the slower propagating PWs are affected significantly by the zonal winds whose seasonal variations change drastically with altitude throughout the region.

IV. Discussion and Conclusion

As we had pointed out earlier (Mayr et al., 2003), waves of the kind described here have been discussed in the classical literature by Longuett Higgins (1968) who classified them as Class I waves. These waves have also been referred to as Inertio Gravity Waves (Volland, 1988; Andrews, Holton, and Leovy, 1990), which is appropriate since the Coriolis force is important for periods close to 12 hours. Due to the action of the Coriolis force, the eastward and westward propagating components are expected to differ significantly. For the m = 1 waves in Longuett Higgins (1968) specifically, the westward components peak at the poles while the eastward components tend to peak at mid latitudes. This is consistent with the numerical results earlier presented. Considering that the waves discussed

here have zonal wavenumbers m = 0 to 4, we refer to them as planetary-scale inertio gravity waves (IGW).

We have shown with Figure 10 that the IGWs still appear in the model when the tidal source is turned off. The waves then differ, also in their seasonal variations. But the periods that are excited and the amplitudes are similar, from this we infer that the tides are not essential to generate the IGWs. That the tides affect the IGWs is not surprising in light of the interactions that can occur, and are known to occur, between the different dynamical components in the mesosphere. A prominent candidate for such interactions is the filtering of small-scale gravity waves (GW) that are parameterized in the NSM, which can produce non-linear coupling between PWs and tides for example. Since the momentum of the GWs is absorbed in wind shears and thus tends to amplify the dynamical features, under conservation of momentum, the theme emerging from our modeling studies has been that there is "no free lunch". Tides thus can be amplified by the GWs at the expense of IGWs or visa versa.

In our NSM, the IGWs are generated by the instabilities that can develop in the zonal mean circulation. When we turn off the solar heating that drives the m = 0 temperature, pressure and wind fields, the IGW disappear, like the PWs. Presently, there is no explicit source in the model to generate PWs or IGWs. As seen from the numerical results presented, and in particular from Figures 8 and 9, the IGWs reveal persistent seasonal variations. Throughout the years, the IGWs tend to be strongest in winter and spring, and they are decidedly weaker during summer months. Although not shown, this pattern in the seasonal variations of the IGWs is prevalent throughout the mesosphere. Such a pattern is also seen in the PWs at altitudes around 60 km (Figure 11) where the waves appear to be largely generated. The apparent similarity between the PWs and IGWs thus gives credence to the suggestion that both classes of waves are generated by similar excitation mechanisms. Plumb (1983) proposed the baroclinic instability for generating the 2-day PWs, and Chan et al. (1994b) suggested that it produced the 4-day wave in their model.

Although the IGWs and PWs appear to have similar roots in the way they are generated, their propagation characteristics in the mesosphere are significantly different. With their low propagation periods and planetary-scale wavelengths, the fast IGWs can propagate through the atmosphere without encountering critical levels. Except for viscous dissipation, the waves thus propagate virtually unattenuated to reach thermospheric altitudes. In contrast, the slower PWs can interact with the zonal circulation. Their oscillation periods are thus modified to change the character of the waves including their seasonal variations. This is apparent for example in the 2-day PWs generated in the NSM, which

are more prevalent at 60 km in the winter hemisphere (Figure 11) but at 90 km in the summer hemisphere (not shown) as observed.

The fast IGW discussed also differ from the slower inertio gravity waves, which make up the long period component of the saturated gravity wave spectrum in the middle atmosphere (Fritts, 1984). Such inertio gravity waves have been observed with radars (e.g., Fritts et al., 1984; Muraoka et al., 1988; Tsuda et al., 1989), and they have horizontal wavelengths between 500 and 3000 km and periods between 5 and 11 hours. These waves thus propagate with velocities that are close to those of the background zonal winds so that they are subject to critical level absorption and dissipation, which is evident from the observed altitude invariance of their amplitudes.

In summary, the IGWs represent a distinct class of waves, which have in common with PWs that they appear to be generated by instabilities, preferentially during the winter and spring season. Relative to the PWs, however, the IGWs generally propagate much faster and thus experience little attenuation. This also applies in relation to the long-period inertio gravity waves that have been observed with much shorter horizontal wavelengths.

In summary, the planetary-scale IGWs discussed are related the Class I waves derived from classical tidal theory (Longuett Higgins, 1968). Except for the excitation mechanism, the waves have the properties of atmospheric diurnal tides. Independent of the tides, however, the IGWs appear in the NSM as a distinct class of waves to some extent similar to the PWs that are generated. Without tidal excitation and in certain seasons, the NSM produces IGWs with a spectrum that contributes significantly to the 12-hour periodicity so that the waves appear like semi-diurnal tides – which is the subject of a separate paper by Talaat et al. (2004).

References

Andrews, D. G., J. R. Holton, and C. B. Leovy, *Middle Atmosphere Dynamics*, Academic Press, Orlando, 1987.

Chan, K. L., H. G. Mayr, J. G. Mengel, and I. Harris, A 'stratified' spectral model for stable and convective atmospheres, *J. Comp. Phys.*, **113**, 165, 1994a.

Chan, K. L., H. G. Mayr, J. G. Mengel, and I. Harris, A spectral approach for studying middle and upper atmospheric phenomena, *J. Atm. Terr. Phys.*, **56**, 1399, 1994b.

Forbes, J. M., N. A. Makarov, Y. I. Portnyagin, First results from the meteor radar at South Pole: A large 12-hour oscillation with zonal wavenumber one, *Geophys. Res. Lett.*, **22**, 3247, 1995.

Fraser, G. J., Summer circulation in the Antarctic middle atmosphere, *J. Atm. Terr. Phys.*, **46**, 143, 1984.

Fritts, D. C., Gravity wave saturation in the middle atmosphere: A review of theory and observations, *Rev. Geophys. Space Phys.*, **22**, 275, 1984.

Fritts, D. C., B. B. Balsley, and W. L. Ecklund, VHF echoes from the arctic mesosphere and lower thermosphere, Part II: Interpretations, in *Dynamics of the Middle Atmosphere*, Eds., J. R. Holton and T. Matsuno, 97, 1984.

Hernandez, G., R. W. Smith, G. J. Fraser, and W. L. Jones, Large-scale waves in the upper mesosphere at antarctic high-latitudes, *Geophys. Res. Lett.*, **19**, 1347, 1992.

Hernandez, G., R. W. Fraser, and Smith, G. J., Mesospheric 12-hour oscillation near south pole antarctica, *Geophys. Res. Lett.*, **20**, 1787, 1993.

Hines, C. O., Doppler-spread parameterization of gravity-wave momentum deposition in the middle atmosphere, 1, Basic formulation, *J. Atmos. Solar Terr. Phys.*, **59**, 371, 1997a.

Hines, C. O., Doppler-spread parameterization of gravity-wave momentum deposition in the middle atmosphere, 2, Broad and quasi monochromatic spectra, and implementation, *J. Atmos. Solar Terr. Phys.*, **59**, 387, 1997b.

Longuett-Higgins, M. S., The eigenfunctions of Laplace's tidal equations over a sphere, *Phi. Trans. Roy. Soc. London*, **A262**, 511, 1968.

Mayr, H. G., J. G. Mengel, K. L. Chan, and H. S. Porter, Seasonal variations of the diurnal tide induced by gravity wave filtering, *Geophys. Res. Lett.*, **25**, 943, 1998.

Mayr, H. G., J. G. Mengel, K. L. Chan, and H. S. Porter, Mesosphere dynamics with gravity forcing: Part II, Planetary waves, *J. Atm. Solar-Terr. Phys.*, **63**, 1865, 2001.

Mayr, H. G., J. G. Mengel, E., R. Talaat, H. S. Porter, and K. L. Chan, Non-migrating tides, with zonally symmetric component, generated in the mesosphere, Paper EAE03-A-03691, presented at EGS-AGU-EUG Joint Assembly, Nice, France, 2003.

Mengel, J. G., Mayr, H. G., Chan, K. L., Hines, C. O., Reddy, C. A., Arnold, N. F., Porter, H. S., Equatorial oscillations in the middle atmosphere generated by small-scale gravity waves, *Geophys. Res. Lett.*, **22** , 3027, 1995.

Muraoka, Y, T. Sugyama, and K. Kawahira, Cause of a monochromatic inertio-gravity wave breaking observed by the MU radar, *Geophys. Res. Lett.*, **15** , 1349, 1988.

Muraoka, Y, S. Fukao, T. Sugyama, M. Yamamoto, T. Nakamuro, T. Tsuda, and S. Kato, Features of a mesospheric inertio-gravity wave observed with the MU radar, *J. Atm. Terr. Phys.*, **56**, 1163, 1994.

Plumb, R. A., Baroclinic instability of the summer mesosphere: A mechanism for the quasi-2-day wave?, *J. Atmos. Sci.*, **40**, 262, 1983.

Tsuda, T., T. Inoue, D. C. Fritts, T. E. VanZandt, S. Kato, T. Sato, and S. Fukao, MST radar observations of a saturated gravity wave spectrum, *J. Atm. Sci.*, **46**, 2440, 1989.

Volland, H., *Atmospheric Tidal and Planetary Waves*, Kluwer Academic Publ., Boston, MA, 1988.

Figure Captions

Figure 1: Time-altitude contour plot of meridional winds for zonal wavenumber m = 1 at 84°N (a) and 77°N (b), Gaussian points, during March (late northern winter) of the 3rd model year, when waves with periods around 10 hours are prominent at polar latitudes. For illustrative purpose, two examples of wave periods are identified from zero intersections. (To reduce output, the model results are recorded with 5 km altitude intervals, which causes the contours to appear ragged.) Horizontal winds at the poles must have zonal wavenumber m = 1, and the analysis shows that the waves there predominantly propagate (rotate) westward. Away from the poles, however, the other wavenumbers also contribute to the oscillations.

Figure 2: Similar to Figure 1 but for m = 0 of temperature variations at 84°N (a) and 70°N (b) and related meridional winds at 77°N (c). Temperature perturbations at the poles must have zonal wavenumber m = 0.

Figure 3: Maximum meridional wind amplitudes of stationary m = 0 wave (a), and eastward (b, c) and westward (d, e) propagating waves (m = 1, 2) for periods from 9 to 10.5 hours, computed with a running window of 15 days from the time span of 26 to 29 months (March through May of the 3rd model year). Contour plots are presented versus height and latitude, applying the Mercator projection to expand the regions at high latitudes where the waves are prominent. The maximum amplitudes are stated in each panel. Note that for m = 1 the westward winds (d) continue to increase towards the poles, in contrast to the eastward waves (b) that peak around 75°N. In the northern hemisphere, in late winter and spring, the amplitudes are much larger than in the southern summer hemisphere.

Figure 4: Similar to Figure 3 but for temperature perturbations. Note that the largest amplitudes (10 K) are generated for m = 0 in the northern polar region.

Figure 5: Maximum amplitude spectra for zonal wavenumbers m = 0 (a), m = 1 (b) and m = 2 (c) at 100 km for periods between 8 and 14 hours, computed from the 26 to 29 months time span (March through May) with a running window of 15 days. The gray scale is used for m = 0 (no propagation), red for westward, and blue for eastward propagation. In (b) and (c), the contour intervals are variable to describe the large migrating and non-migrating tides. Note the non-migrating semi-diurnal tide (12-hour period) at m = 1 that peaks at the poles (b), which is produced in the NSM through non-linear interaction between the solar driven semi-diurnal migrating tide and stationary m = 1 planetary waves as Forbes et al. (1995) had proposed. The x-marks on the vertical axes denote the discrete periods for which the amplitudes are computed to produce the contours. By casting for the analysis a relatively large time span of 3 months, the different wave periods in the spectra are usually not excited simultaneously. Note again the westward waves that increase towards the poles, and the eastward waves that peak at lower latitudes.

Figure 6: Similar to Figure 5 but for temperature perturbations. For m = 0 (a), the temperature amplitudes peak at the poles and are larger for the 9-hour wave than the non-migrating semi-diurnal tide (12 hours).

Figure 7: Snap-shots of the meridional winds in the southern hemisphere near 32.5 months (mid September), when the waves are most prominent. The winds are derived from short time spans of 3 days for 9- hour westward and eastward propagating waves. (Recorded with 5 km intervals, the contours appear ragged.) The characteristic differences between the eastward and westward propagating components are evident, each revealing horizontal wavelengths of about 40° latitude. The vertical wavelength is about 25 km. With phase intervals of 3 hours, the waves are shown progressing downwards.

Figure 8: To characterize the seasonal and latitudinal variations in the meridional winds at 100 km, wave amplitudes are shown for the stationary waves with m = 0 (a), and the eastward (a) and westward (b) propagating m = 1 components. For periods between 9 and 10.5 hours, a moving window of 15 days is applied. Maximum (and minimum) amplitudes (m/s) are stated, i.e., 17.5 (a), 15.6 (b) and 26.8 (c). In contrast to westward waves that peak at poles, the eastward waves do not extend into the polar regions but are more prevalent at mid to low latitudes. Largest amplitudes occur preferentially during late winter and spring, and this pattern prevails throughout the mesosphere. The seasonal variations for the waves with m = 2, 3 and 4 (not shown) reveal similar trends except that they vanish at poles.

Figure 9: Like Figure 8 but for temperature variations with maximum amplitudes (K): 6 (a), 4.7 (b), 5.7 (c).

Figure 10: Similar to Figure 8 but computed without excitation of the westward propagating diurnal and semi-diurnal tides. The seasonal variations are different, but the amplitudes have comparable magnitudes to indicate that the tides are not essential to generate the waves.

Figure 11: Computed seasonal variations of meridional winds at 60 km for planetary waves with zonal wave numbers m = 1 and 3. The resemblance with the seasonal variations of the waves in Figure 8 indicates that both classes of waves are generated by the same excitation source, presumably convective instability as proposed in the literature.

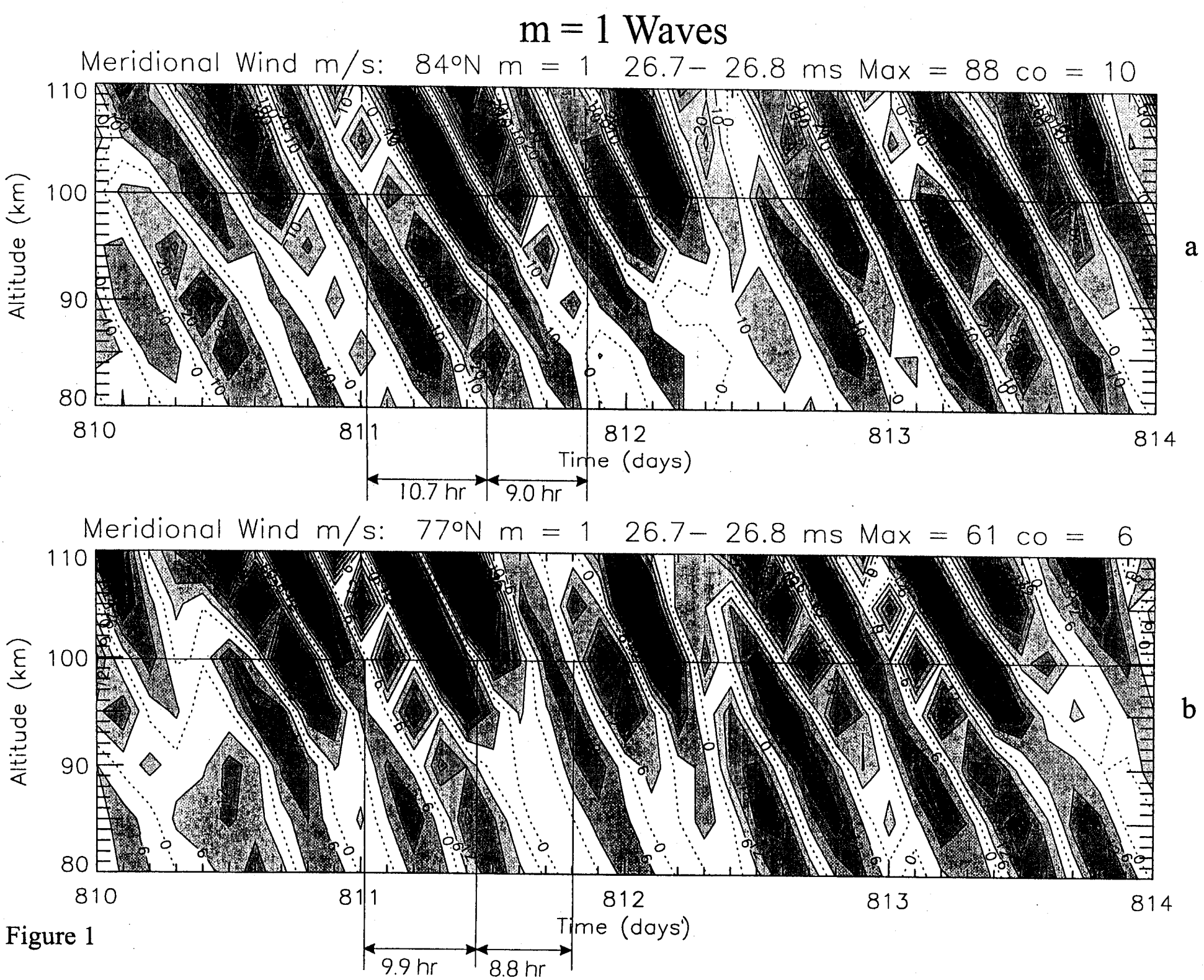
m = 1 Waves
Meridional Wind m/s: 84°N m = 1 26.7– 26.8 ms Max = 88 co = 10
Altitude (km)
110
100
90
80
810
811
812
813
814
Time (days)
10.7 hr
9.0 hr
a
Meridional Wind m/s: 77°N m = 1 26.7– 26.8 ms Max = 61 co = 6
Altitude (km)
110
100
90
80
810
811
812
813
814
Time (days)
9.9 hr
8.8 hr
b

Figure 1

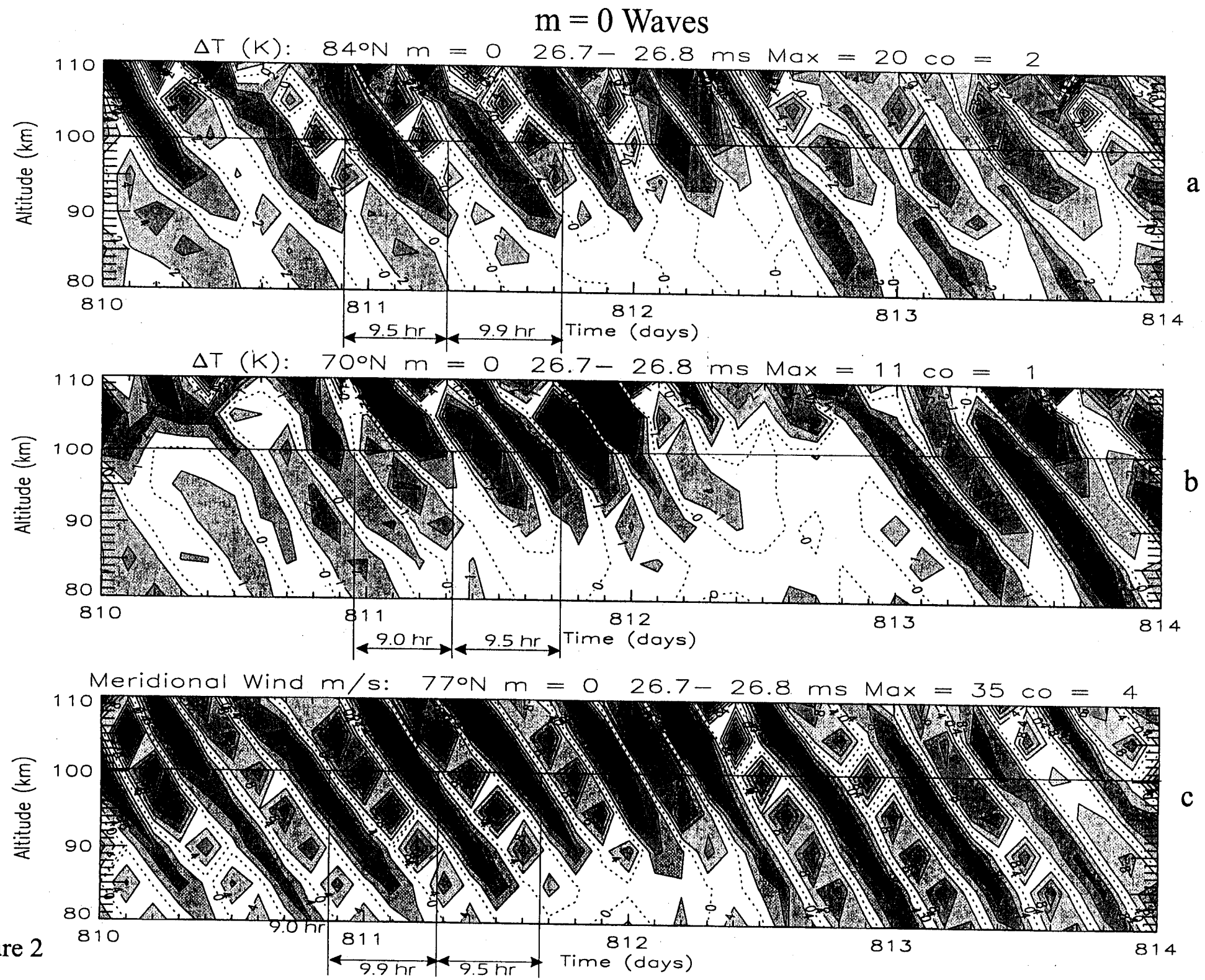
m = 0 Waves
ΔT (K): 84°N m = 0 26.7– 26.8 ms Max = 20 co = 2
Altitude (km)
110
100
90
80
810
811
812
813
814
9.5 hr
9.9 hr
Time (days)
a
ΔT (K): 70°N m = 0 26.7– 26.8 ms Max = 11 co = 1
9.0 hr
9.5 hr
b
Meridional Wind m/s: 77°N m = 0 26.7– 26.8 ms Max = 35 co = 4
9.0 hr
9.9 hr
9.5 hr
c

Figure 2

Meridional Wind

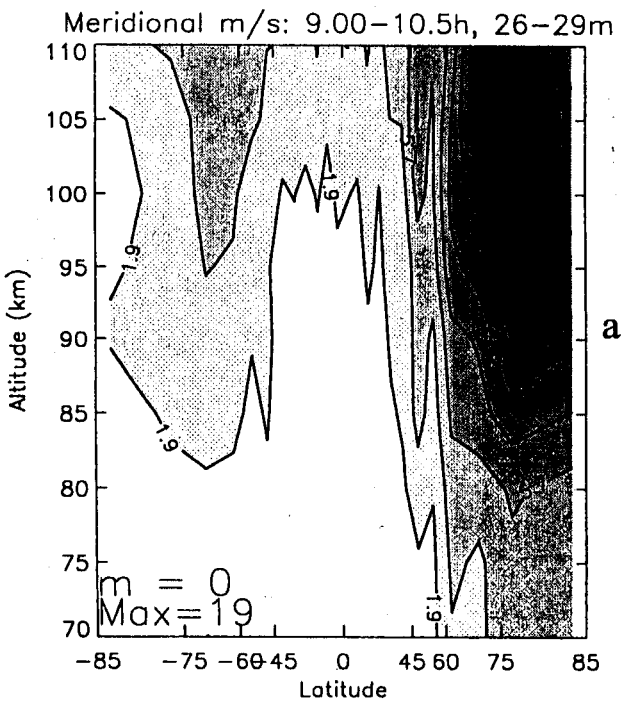

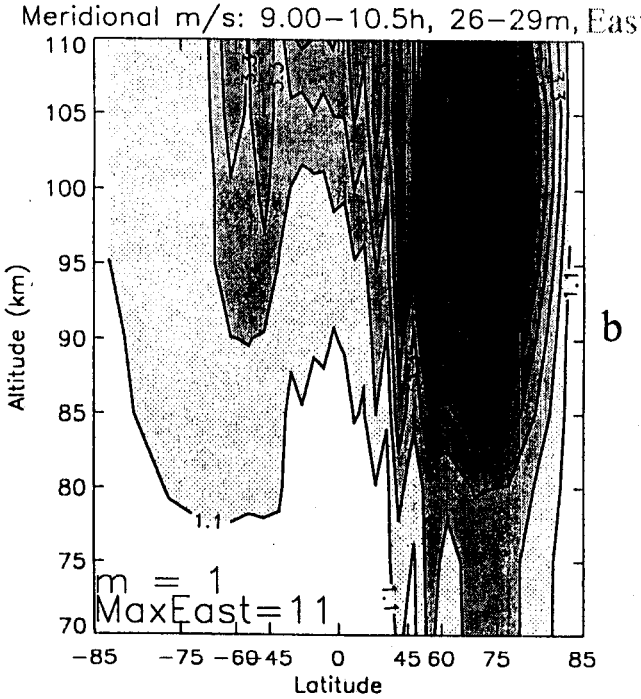

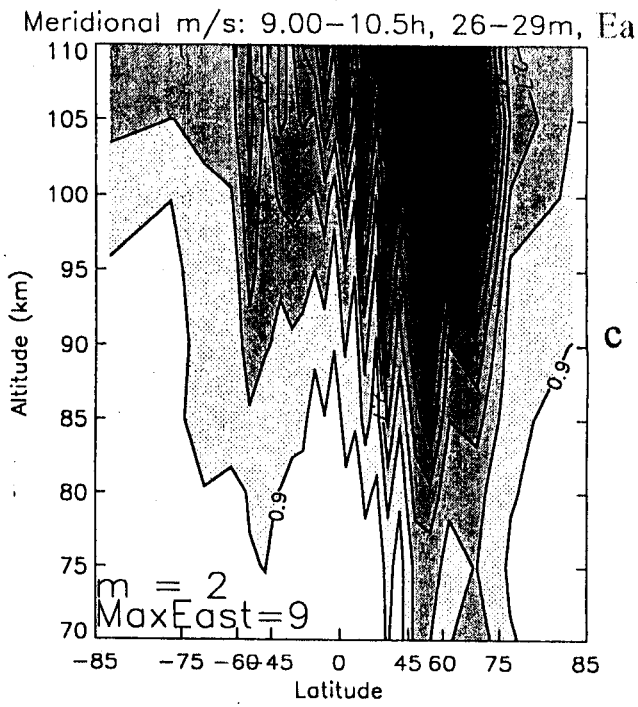

cut=1 window=15 ndpa,ndpb=40 34 fac=1 C495

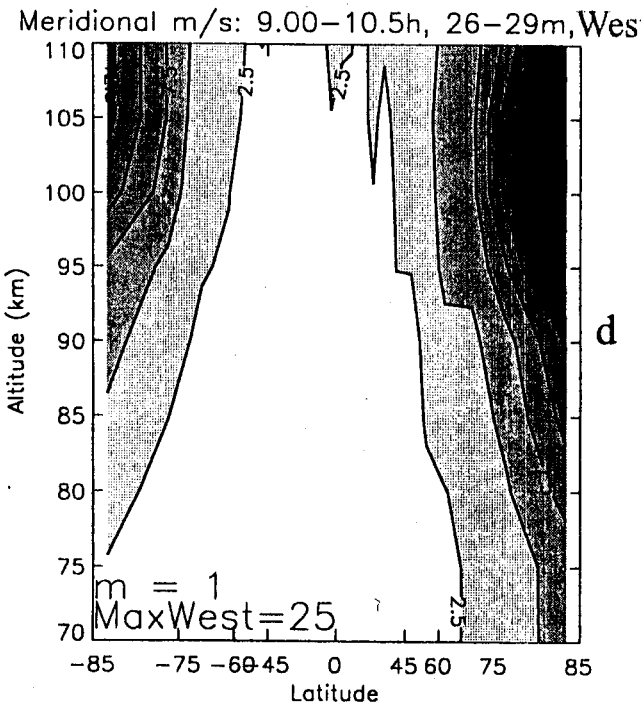

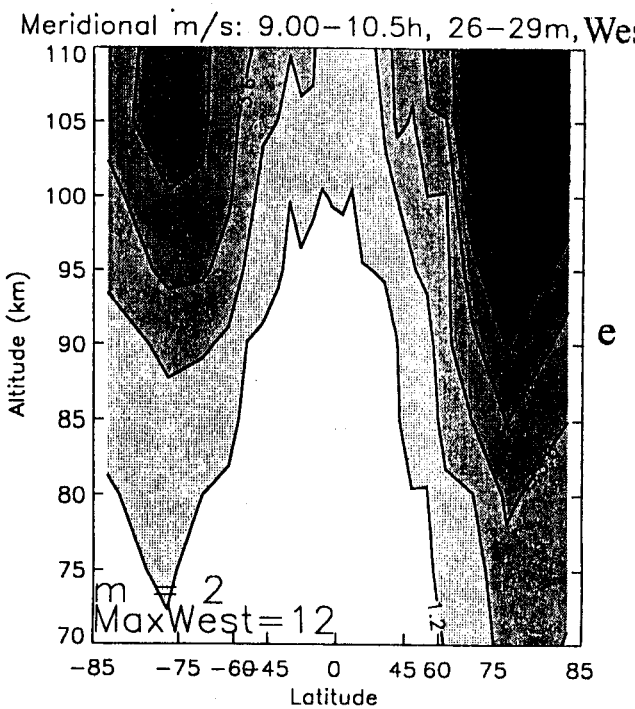

cut=1 window=15 ndpa,ndpb=40 34 fac=1 C496

Figure 3

Temperature Perturbation

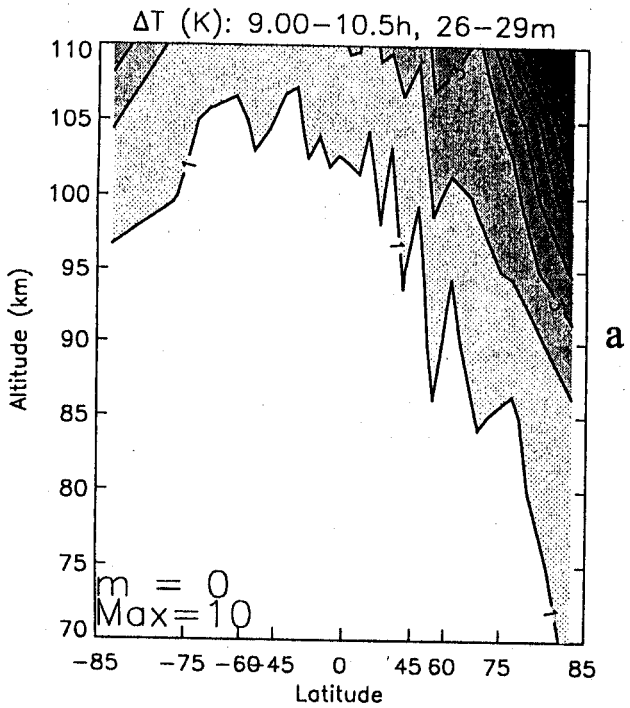

a

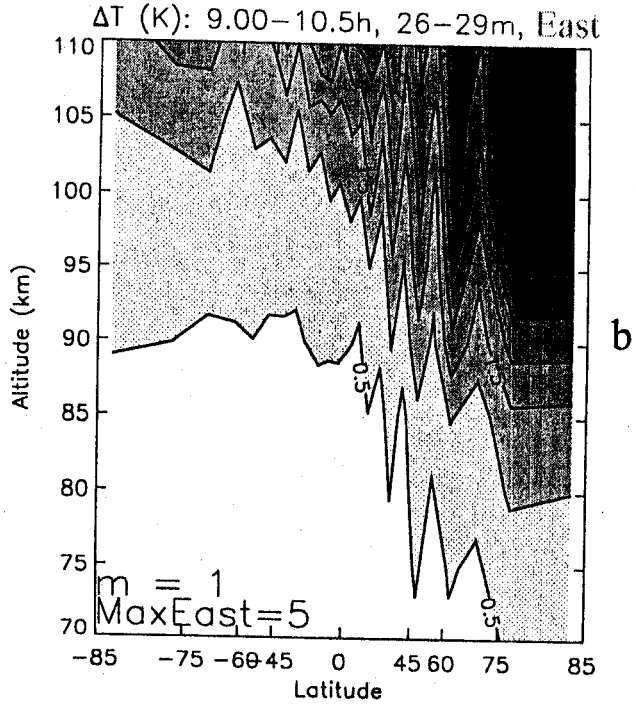

b

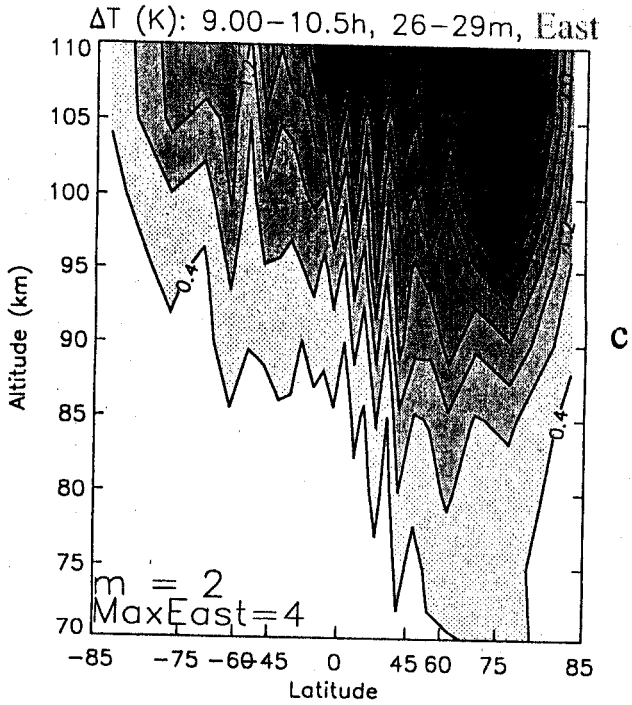

c

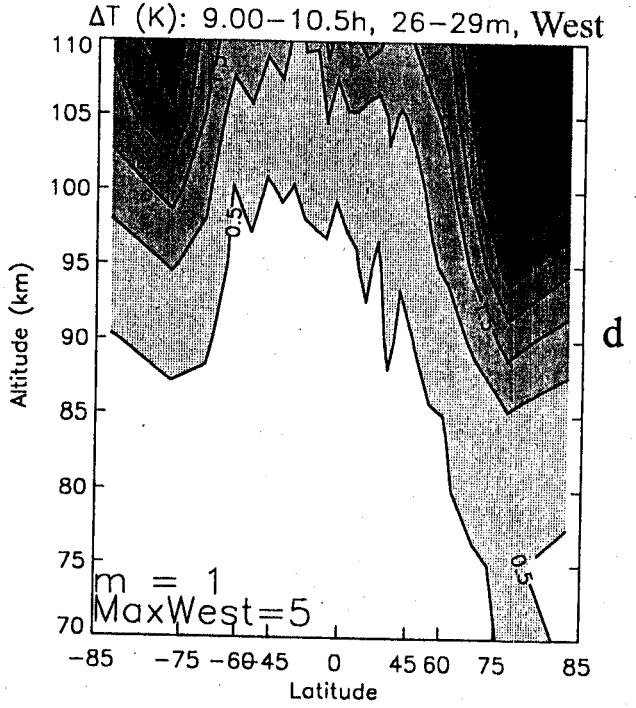

d

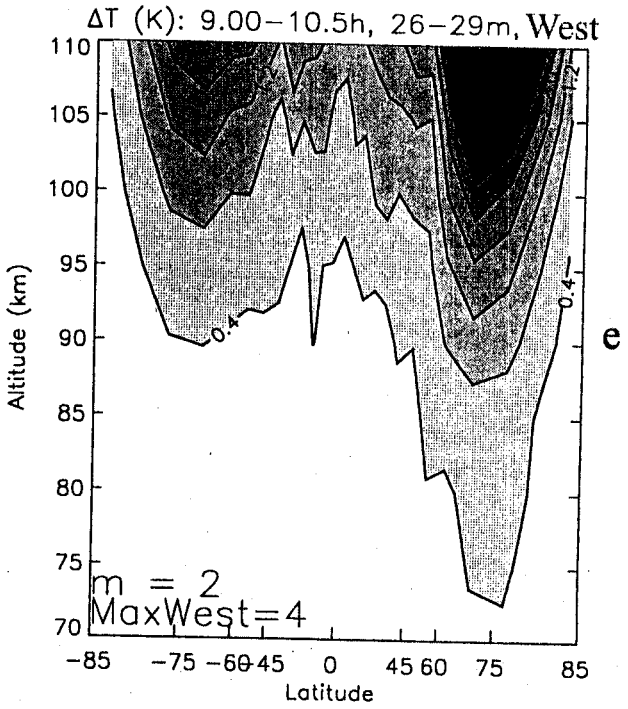

e

Figure 4

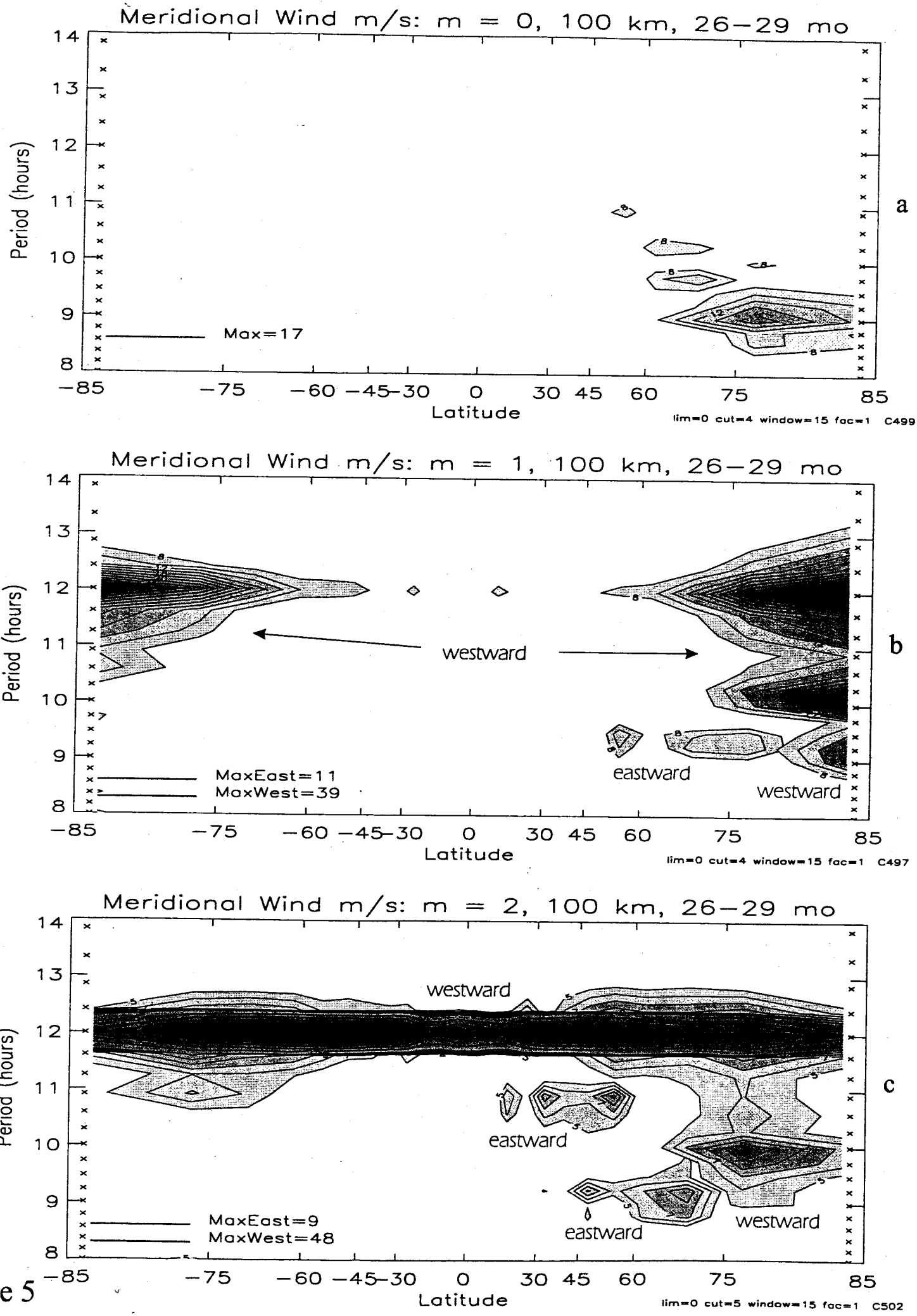
Meridional Wind m/s: m = 0, 100 km, 26–29 mo
Period (hours)
Latitude
Max=17
a
lim=0 cut=4 window=15 fac=1 C499
Meridional Wind m/s: m = 1, 100 km, 26–29 mo
westward
eastward
westward
MaxEast=11
MaxWest=39
b
lim=0 cut=4 window=15 fac=1 C497
Meridional Wind m/s: m = 2, 100 km, 26–29 mo
westward
eastward
eastward
westward
MaxEast=9
MaxWest=48
c
lim=0 cut=5 window=15 fac=1 C502

Figure 5

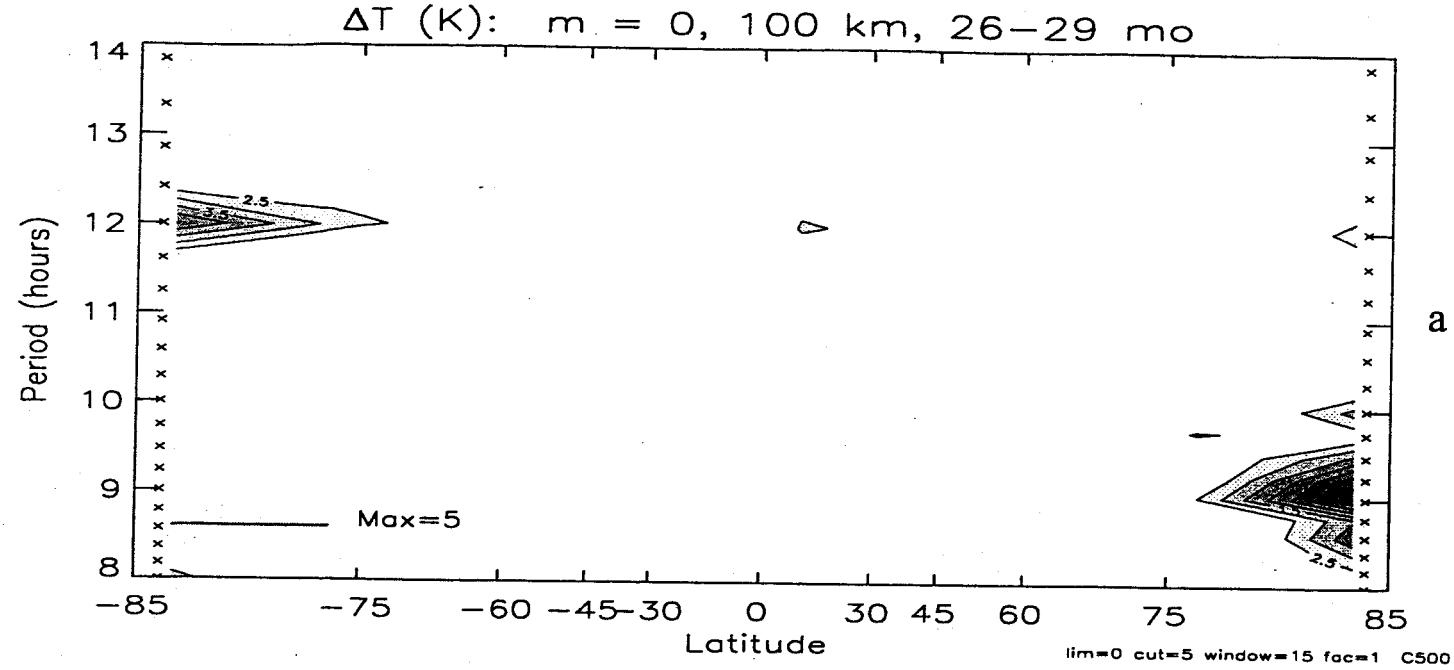
ΔT (K): m = 0, 100 km, 26–29 mo
Period (hours)
Latitude
Max=5
lim=0 cut=5 window=15 fac=1 C500

a

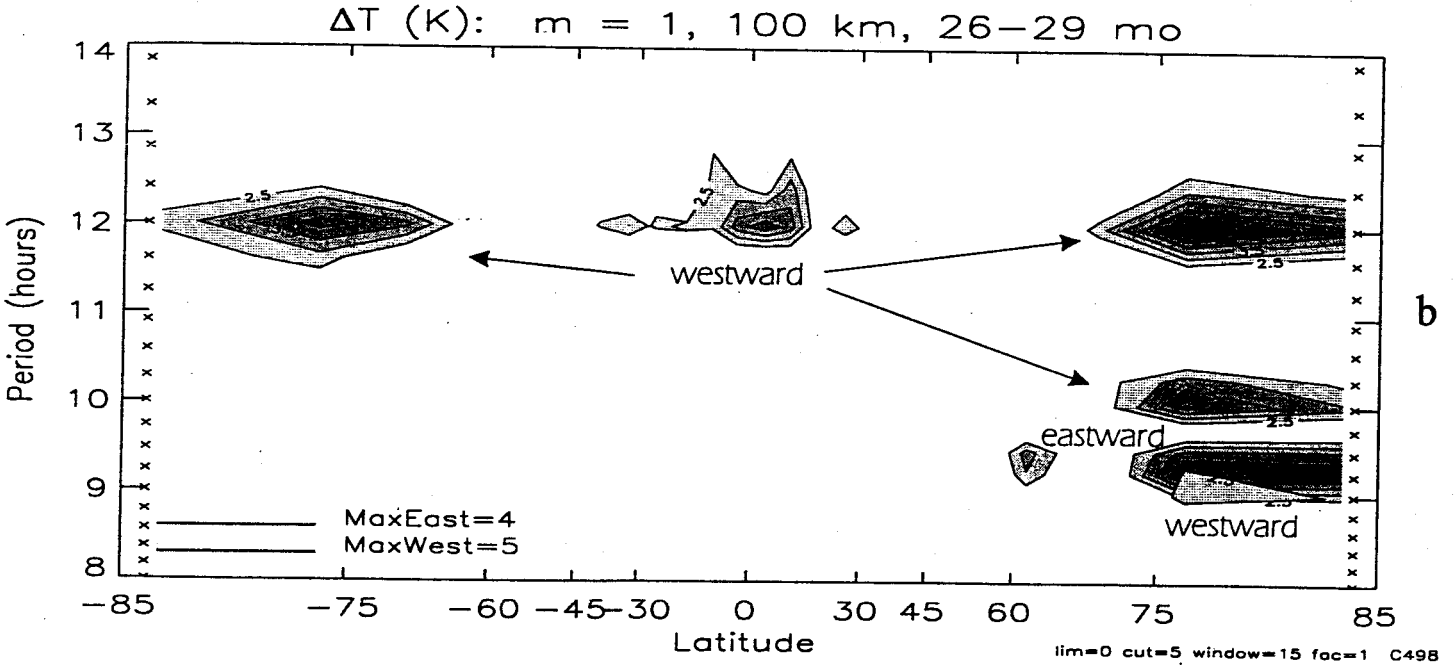
ΔT (K): m = 1, 100 km, 26–29 mo
Period (hours)
Latitude
westward
eastward
westward
MaxEast=4
MaxWest=5
lim=0 cut=5 window=15 fac=1 C498

b

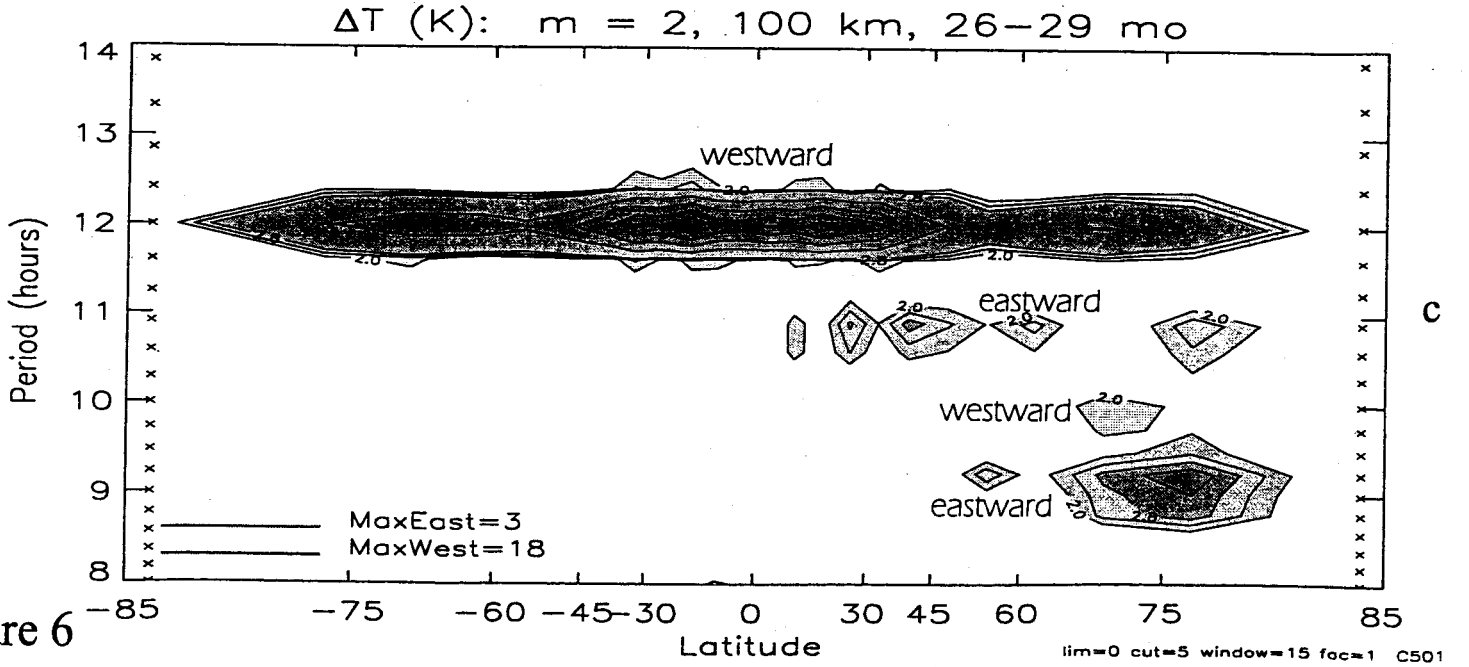
ΔT (K): m = 2, 100 km, 26–29 mo
Period (hours)
Latitude
westward
eastward
westward
eastward
MaxEast=3
MaxWest=18
lim=0 cut=5 window=15 fac=1 C501

c

Figure 6

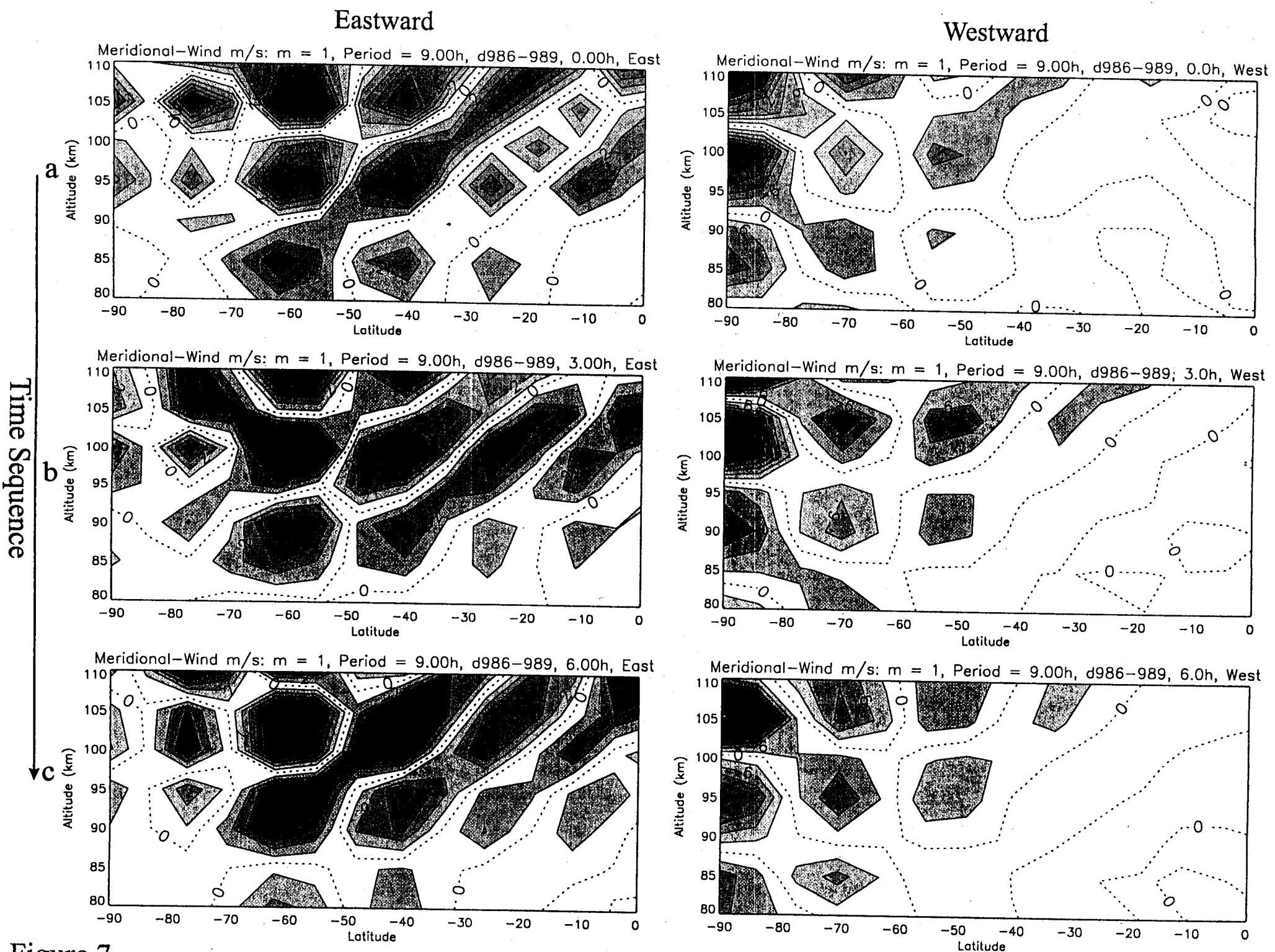

Figure 7

C546

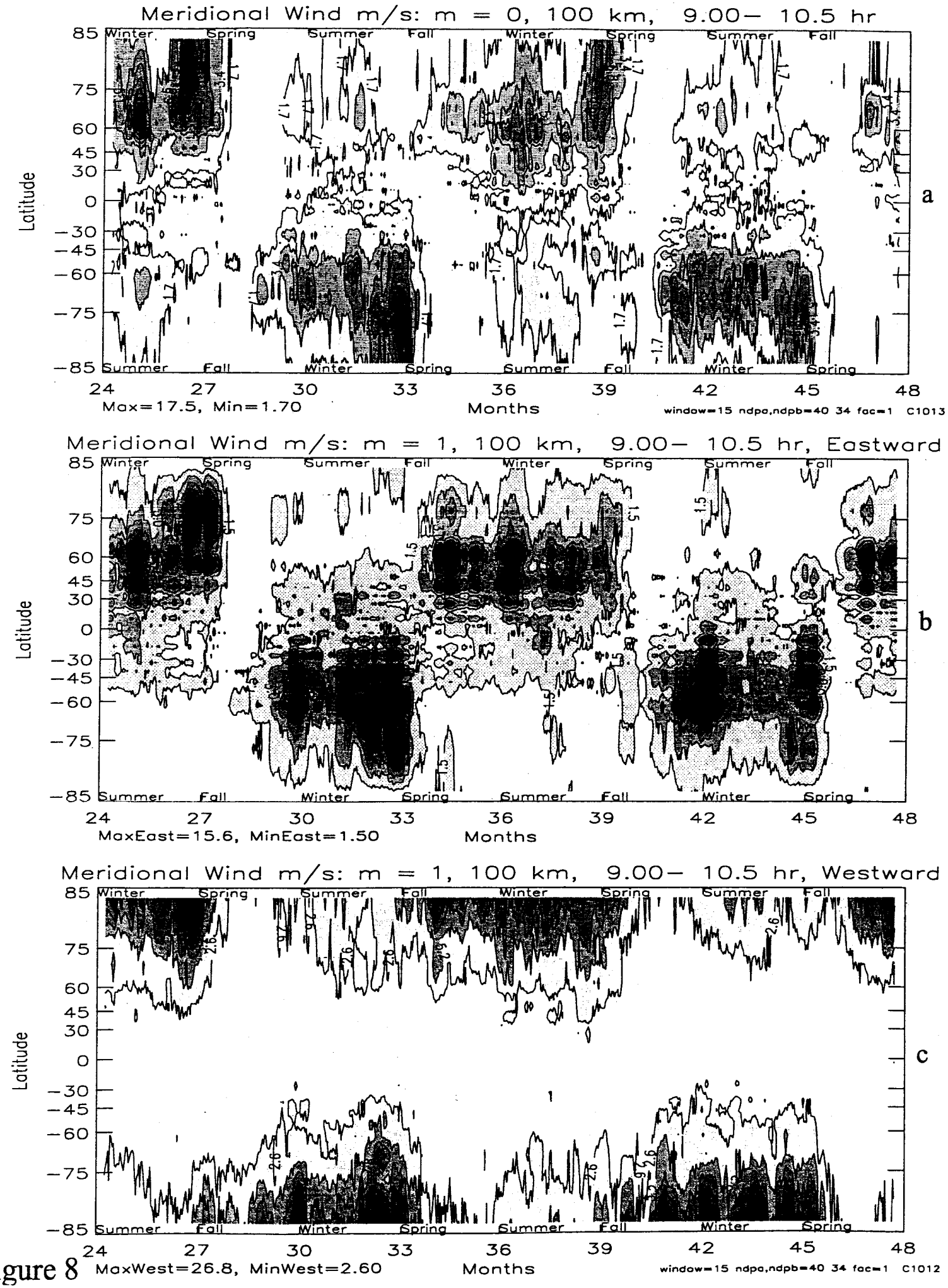
Meridional Wind m/s: m = 0, 100 km, 9.00– 10.5 hr
Winter Spring Summer Fall Winter Spring Summer Fall
Summer Fall Winter Spring Summer Fall Winter Spring
Latitude
85 75 60 45 30 0 −30 −45 −60 −75 −85
24 27 30 33 36 39 42 45 48
Max=17.5, Min=1.70
Months
window=15 ndpa,ndpb=40 34 fac=1 C1013
a
Meridional Wind m/s: m = 1, 100 km, 9.00– 10.5 hr, Eastward
Winter Spring Summer Fall Winter Spring Summer Fall
Summer Fall Winter Spring Summer Fall Winter Spring
Latitude
85 75 60 45 30 0 −30 −45 −60 −75 −85
24 27 30 33 36 39 42 45 48
MaxEast=15.6, MinEast=1.50
Months
b
Meridional Wind m/s: m = 1, 100 km, 9.00– 10.5 hr, Westward
Winter Spring Summer Fall Winter Spring Summer Fall
Summer Fall Winter Spring Summer Fall Winter Spring
Latitude
85 75 60 45 30 0 −30 −45 −60 −75 −85
24 27 30 33 36 39 42 45 48
MaxWest=26.8, MinWest=2.60
Months
window=15 ndpa,ndpb=40 34 fac=1 C1012
c

Figure 8

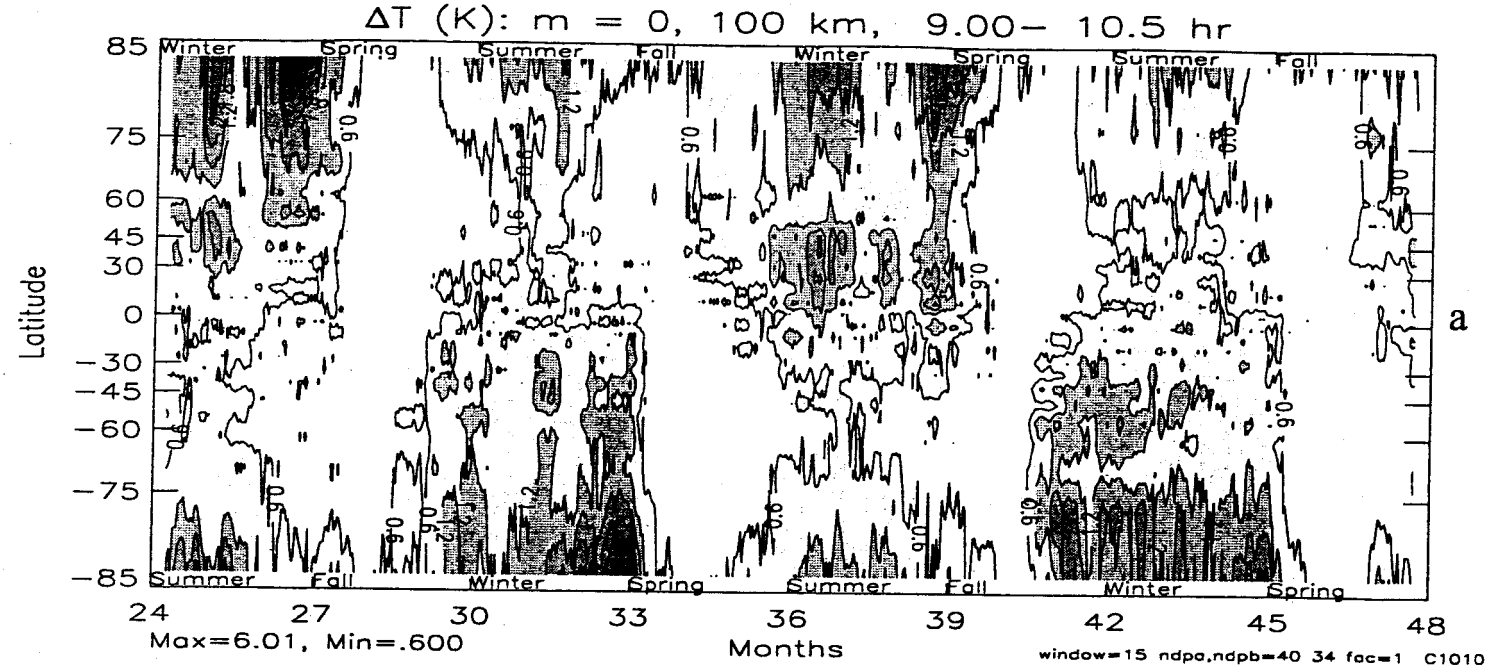
ΔT (K): m = 0, 100 km, 9.00– 10.5 hr
Winter Spring Summer Fall Winter Spring Summer Fall
Latitude
85 75 60 45 30 0 −30 −45 −60 −75 −85
Summer Fall Winter Spring Summer Fall Winter Spring
24 27 30 33 36 39 42 45 48
Max=6.01, Min=.600
Months
window=15 ndpa,ndpb=40 34 fac=1 C1010
a

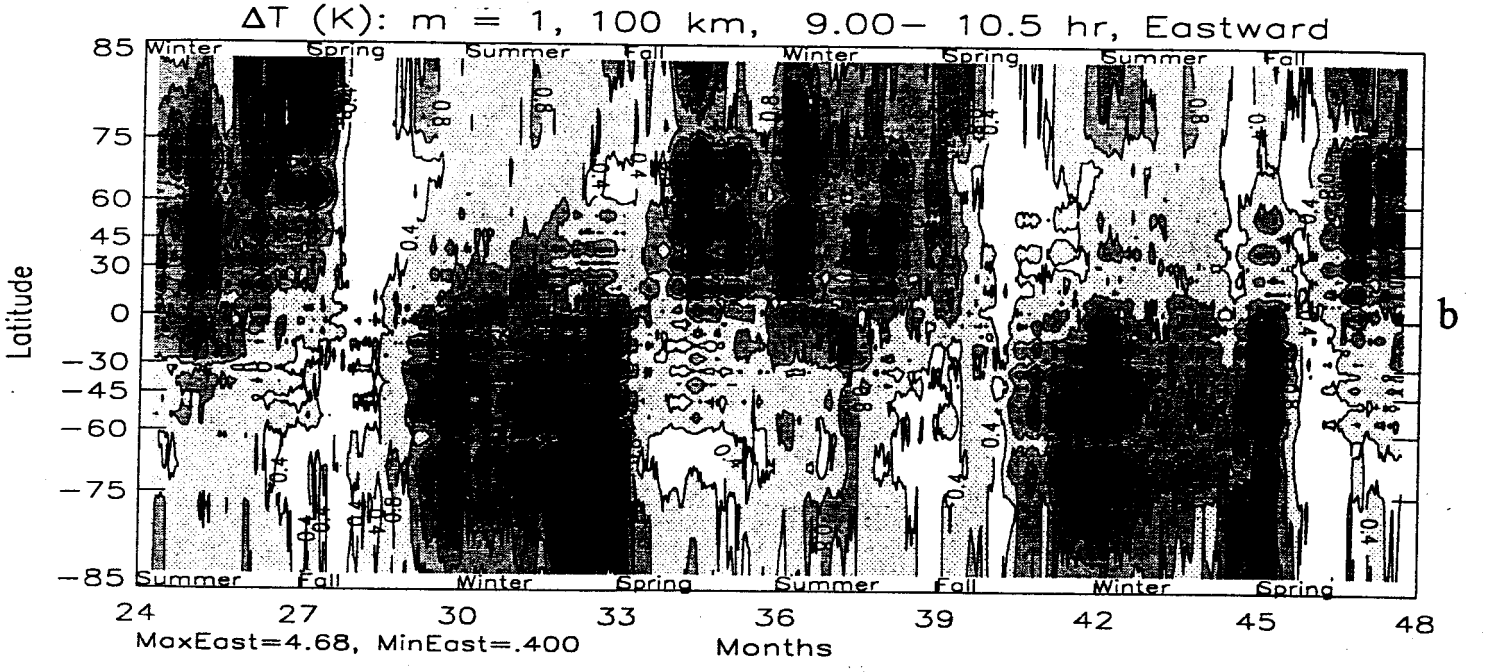
ΔT (K): m = 1, 100 km, 9.00– 10.5 hr, Eastward
Winter Spring Summer Fall Winter Spring Summer Fall
Latitude
85 75 60 45 30 0 −30 −45 −60 −75 −85
Summer Fall Winter Spring Summer Fall Winter Spring
24 27 30 33 36 39 42 45 48
MaxEast=4.68, MinEast=.400
Months
b

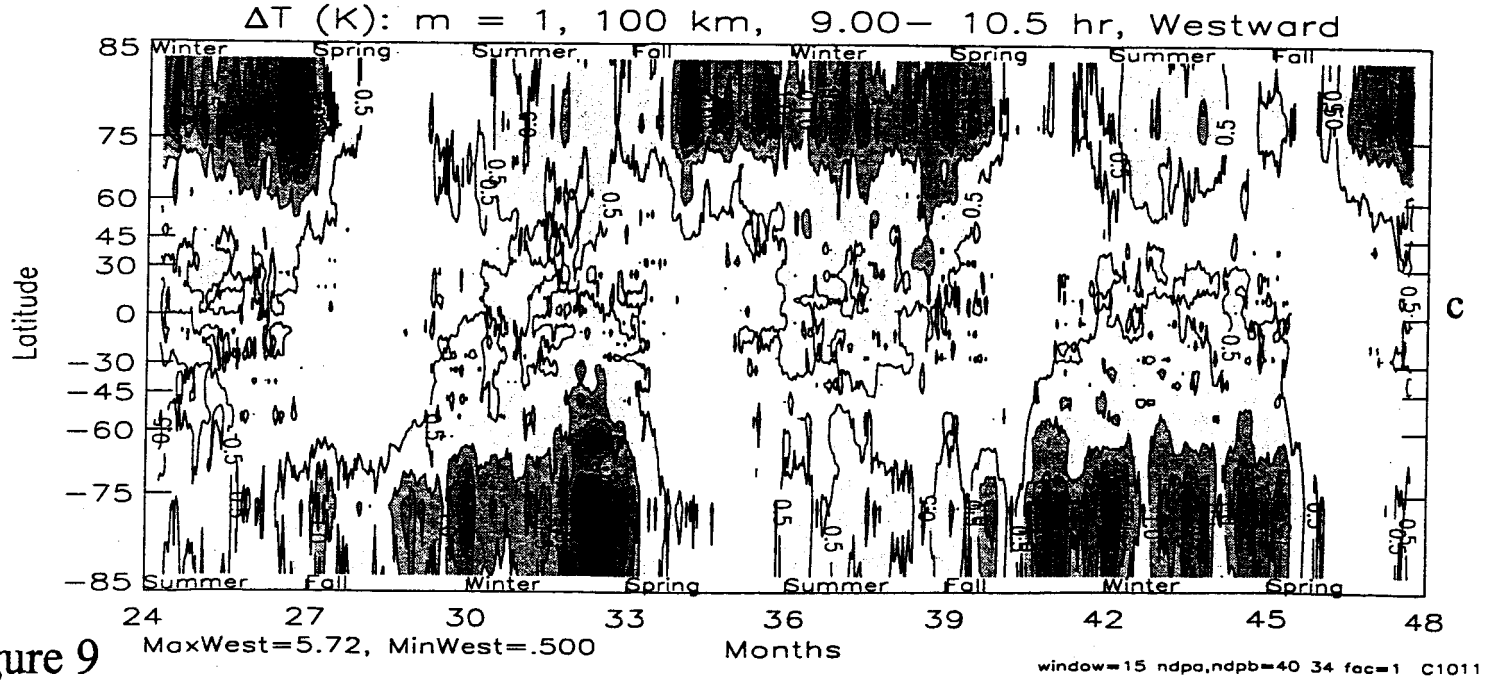
ΔT (K): m = 1, 100 km, 9.00– 10.5 hr, Westward
Winter Spring Summer Fall Winter Spring Summer Fall
Latitude
85 75 60 45 30 0 −30 −45 −60 −75 −85
Summer Fall Winter Spring Summer Fall Winter Spring
24 27 30 33 36 39 42 45 48
MaxWest=5.72, MinWest=.500
Months
window=15 ndpa,ndpb=40 34 fac=1 C1011
c

Figure 9

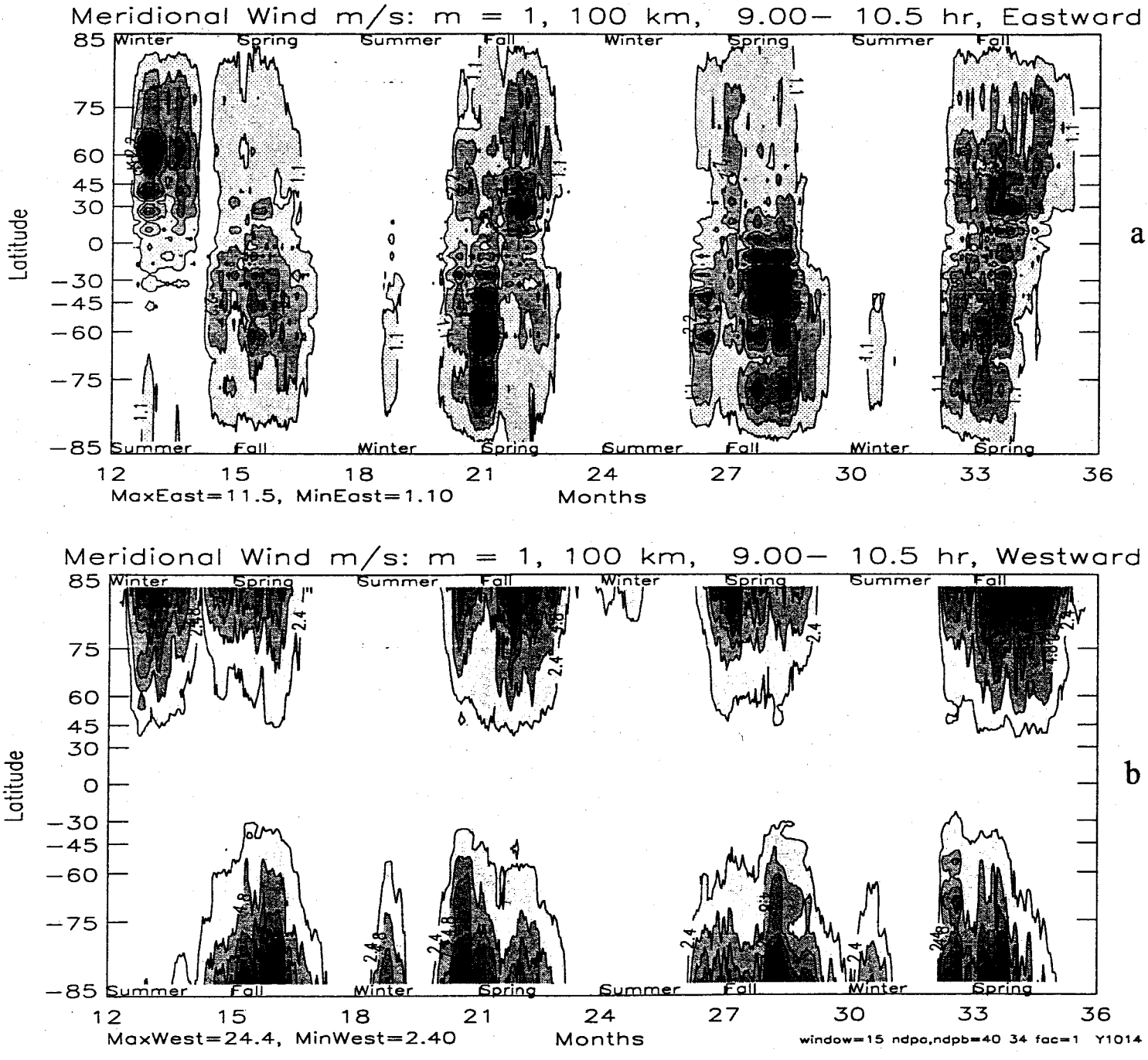
Meridional Wind m/s: m = 1, 100 km, 9.00– 10.5 hr, Eastward
Winter
Spring
Summer
Fall
Latitude
85
75
60
45
30
0
−30
−45
−60
−75
−85
12
15
18
21
24
27
30
33
36
MaxEast=11.5, MinEast=1.10
Months
a
Meridional Wind m/s: m = 1, 100 km, 9.00– 10.5 hr, Westward
MaxWest=24.4, MinWest=2.40
window=15 ndpa,ndpb=40 34 fac=1 Y1014
b

Figure 10

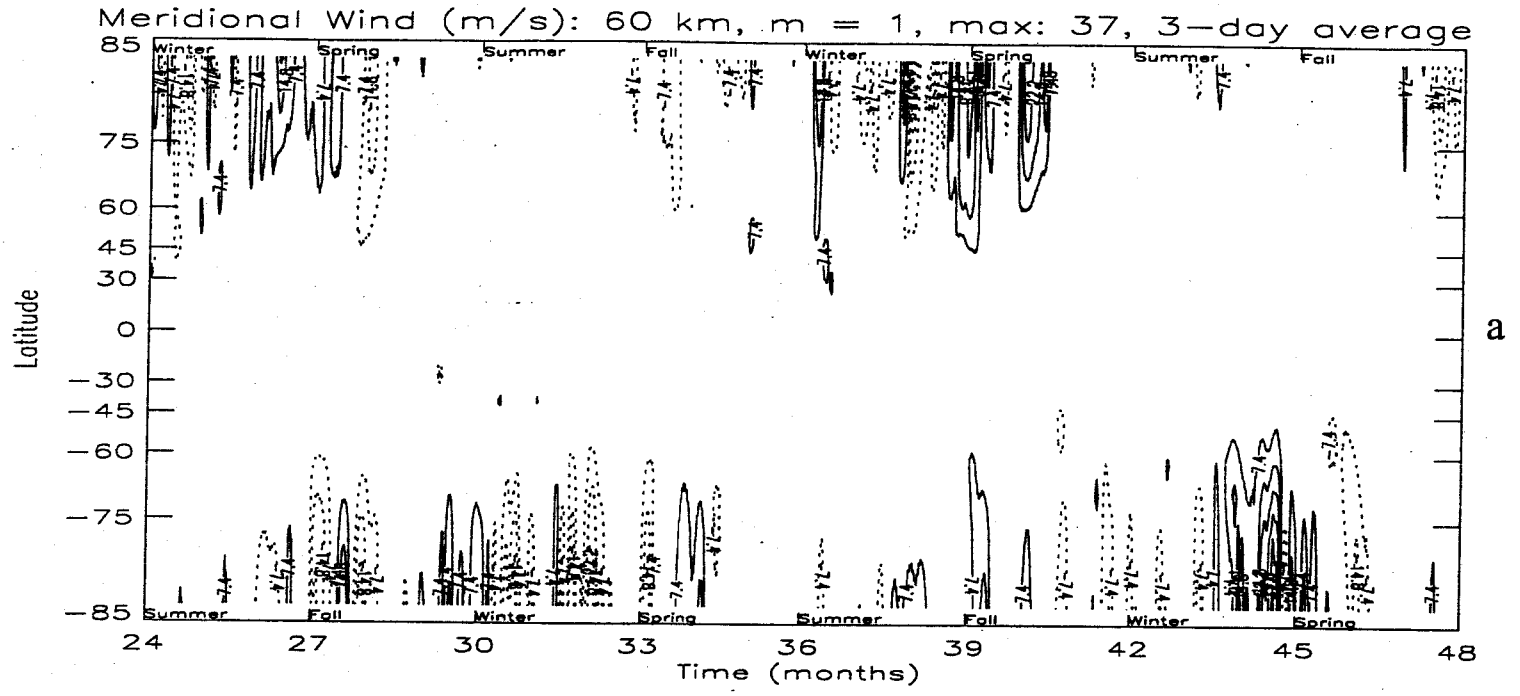
Meridional Wind (m/s): 60 km, m = 1, max: 37, 3—day average
Latitude
Time (months)
Winter
Spring
Summer
Fall
85
75
60
45
30
0
−30
−45
−60
−75
−85
24
27
30
33
36
39
42
45
48

a

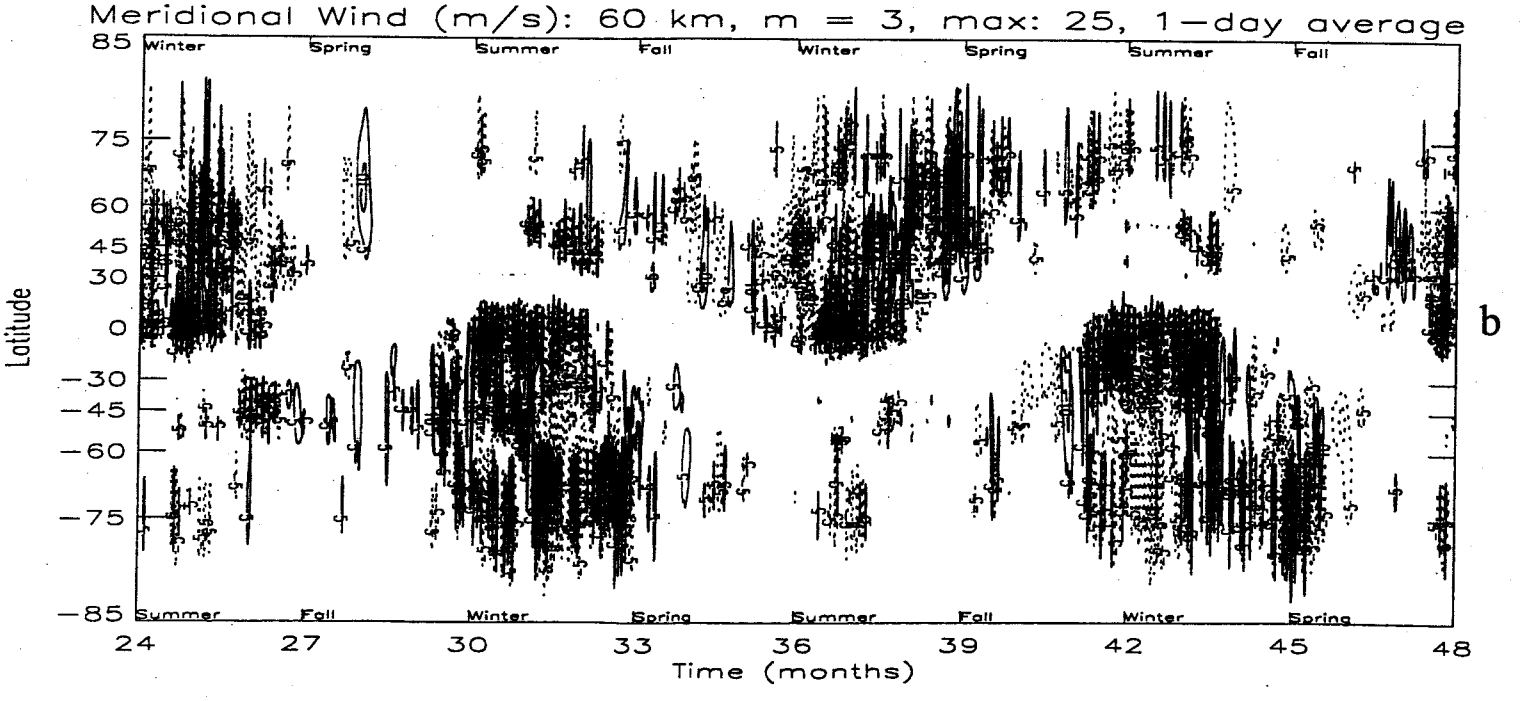
Meridional Wind (m/s): 60 km, m = 3, max: 25, 1—day average
Latitude
Time (months)
Winter
Spring
Summer
Fall
85
75
60
45
30
0
−30
−45
−60
−75
−85
24
27
30
33
36
39
42
45
48

b

Figure 11